IN-SITU X-RAY CHARACTERIZATION OF $LiMn_2O_4$: A COMPARISON OF STRUCTURAL AND ELECTROCHEMICAL BEHAVIOR

MARK A. RODRIGUEZ, DAVID INGERSOLL, & DANIEL H. DOUGHTY
PO Box 5800, Sandia National Laboratories, Albuquerque, NM 87185-1405

ABSTRACT

$Li_xMn_2O_4$ materials are of considerable interest in battery research and development. The crystal structure of this material can significantly affect electrochemical performance. The ability to monitor changes of crystal structure during use, that is during electrochemical cycling, would prove useful to verify and control such structural changes. We report in-situ XRD measurements of $LiMn_2O_4$ cathodes with the use of an electrochemical cell designed for in-situ X-ray analysis. Cells prepared using this cell design allow investigation of the changes in the $LiMn_2O_4$ structure during charge and discharge. We describe the variation in lattice parameters along the voltage plateaus and consider the structural changes in terms of the electrochemical results on each cell. Kinetic effects of $LiMn_2O_4$ phase changes are also addressed. Applications of the in-situ cell to other compounds such as $LiCoO_2$ cathodes and carbon anodes are presented as well.

INTRODUCTION

A large number of highly applied electrochemical systems, *e.g.* batteries, employ crystalline materials. Examples include electrolytic MnO_2 used in alkaline cells, $LiCoO_2$ found in lithium ion rechargeable cells, and Zn/ZnO found in a number of cell chemistries.[1] The performance of many of these materials is highly dependent on their crystal structure. For example, only the spinel polymorph of $LiMn_2O_4$ exhibits a 4V and a 3V plateau, each of which have theoretical capacities of 148 mAh/g. However, the spinel structure does not appear stable along the 3V plateau. The ability to monitor the changes of the crystal structure during electrochemical cycling should prove useful to verify these types of structural changes, as well as aid in the development of structure-activity relationships. Furthermore, the ability to perform the measurements in a cell configuration that allows for use of an electrode structure similar to or identical to that employed in commercial devices has the potential to make significant impact on future cell development. Finally, the ability to monitor these changes in real time could provide useful insight into the dynamics of the system.

The choice of material used to contain the cell or to serve as a window into the cell exerts a significant effect on the overall performance of the final device. For example, Richard, *et. al.*[2] recently described an *in-situ* XRD cell containing a system based on the Ultralife gel technology. In this experimental setup a beryllium window was used in close proximity to the cathode electrode material. Consequently, the window was required to be physically separated from the electrode and electrolyte, in this case by aluminum spacers, to ensure that it did not participate in the electrochemical reactions. In fact, as described, only the gel system could be used in this cell

DISCLAIMER

since liquid electrolyte would lead to wetting of the beryllium window and allow its subsequent participation in the redox reactions. Over 20 diffraction peaks are seen from the cell components themselves over the 2θ range studied. This number of artifact diffraction peaks makes observation of the diffraction pattern from the sample of interest problematic at best. Additionally, very long data acquisition times are required (on the order of 12 hours) for a single pattern. This severely limits real-time data collection on samples to only the slowest charge or discharge rates.

For *in-situ* XRD electrochemical studies, the material used for housing the cell must meet several criteria. First, it must be relatively transparent to the X-ray radiation so as to minimize the absorption of both the incident and diffracted rays. Second, it should have few if any diffraction lines at, or near angles where the sample diffracts. Third, it should be chemically stable to the solvent system utilized, as well as when in contact with the electrode materials. Fourth, it must be electrochemically stable and preferably inert, so as not to interfere with the electrochemical characteristics of the active electrode materials. Fifth, it should be impervious to the solvent system utilized so it will not dry out during the course of the experiment. Sixth, the mechanical characteristics of the material should be such that compression can be applied to the cell to ensure good electrical contact and minimum interfacial resistance. Finally, a method of sealing the cell material to itself and other materials, such as the electrical feedthroughs, must be available. The two materials that were selected for the in-situ cell were polypropylene and polyethylene (1mil thickness).

In order to determine unit cell parameters, high quality X-ray data must be collected. This seemingly simple requirement is not so easily met in an electrochemical cell primarily due to the fact that the electrode can and usually does swell after cell activation and upon charging and discharging. As a result of this swelling the electrode surface can move out of the focal plane of the X-ray source. This movement will likely result in displacement of the diffracted energy and incorrect determination of cell parameters. In the system described here, an internal standard is present that ensures precise determination of the diffraction angles and hence the unit cell parameters.

EXPERIMENTAL

Cell Design

Porous electrodes were prepared and consisted of 83% active material, 8% Teflon used as a binder, and the balance as carbon. The electrodes were prepared using a standard mixing, knead, and roll technique. The final electrode thickness was 11 mil and was approximately 50% porous. The active material used was $LiMn_2O_4$ obtained from FMC and Chemetals and $LiCoO_2$ obtained from FMC. The porous electrodes were pressed into an aluminum current collector grid in such a way that the aluminum grid and porous electrode are at the same height. In this way the aluminum grid served as the internal standard for all XRD measurements. Lithium metal was used as the negative electrode for these studies and was pressed onto a nickel grid which served as the

current collector. A 1 mil Celgard separator was used in these cells. The supporting electrolyte solution used was 1M $LiPF_6$ in ethylene carbonate/diethylene carbonate (70:30). The 12 cm^2 electrodes (6cm X 2cm) were assembled into a stack and placed into a small plastic bag constructed using 1 mil polypropylene (or polyethylene). The bag was assembled by impulse heating of the materials. The current collectors were also sealed to the bag assembly using impulse heating. The cell was then vacuum filled with the electrolyte through a small fill hole left in the cell, and allowed to soak for approximately 5 minutes. At the end of this time period the cell was sealed while a vacuum was applied, thus ensuring compression on the cell components. A picture of the cell dis-assembled into its various parts and fully assembled is shown in Figure 1.

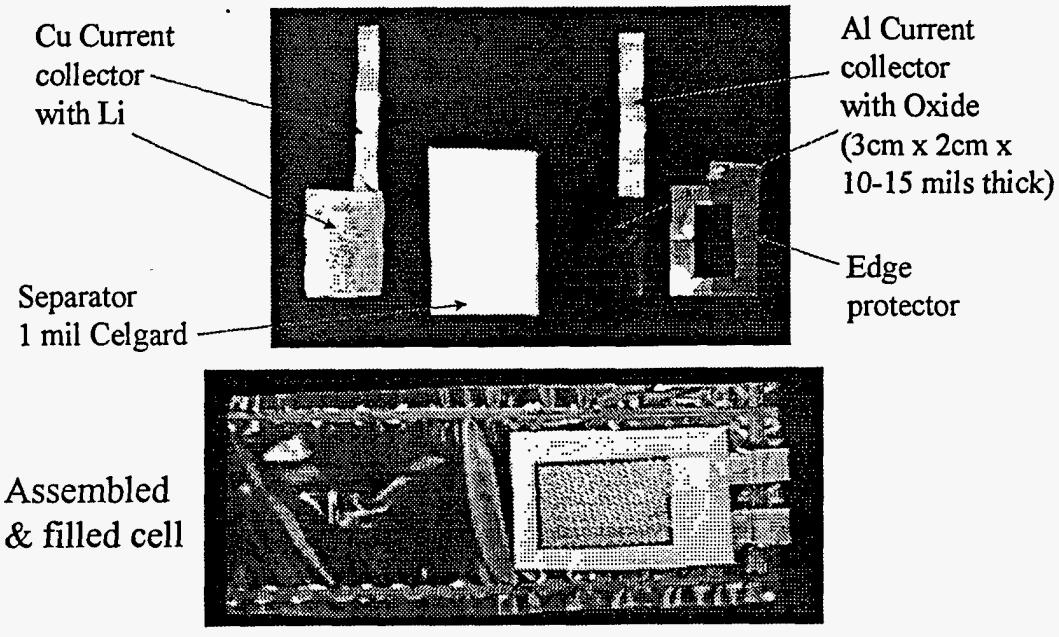

Figure 1. In-situ cell dis-assembled into its respective parts and fully assembled within polyethylene bag.

XRD Data Collection

In-situ measurements can be classified into two categories, *static* or *dynamic* measurements.[3] The varying parameter of interest in this investigation is voltage. In the case of a static in-situ measurement, data is collected on a sample cell at constant voltage. In this type of measurement, the cell is brought to a specific voltage value and held for a long time to reach a relatively equilibrated state. During this time the current is allowed to decay to its equilibrium value. The diffraction pattern is then collected on this sample. For the static measurement the scan speed is not a critical issue since the structure should not be changing appreciably during the analysis, so scan rates tended to be slower to improve the data quality. In a dynamic measurement the voltage is constantly varied while the cell is being processed. In this scenario the scan speed for data collection is much more important. In order to obtain useful information, the rate of data

collection for a pattern should be much faster than changes occurring in structure of the lattice. This important issue for the dynamic experiments required modification to smaller 2θ ranges and shorter counting times.

All XRD patterns were collected using a Siemens automated θ–θ powder diffractometer equipped with Cu Kα radiation, a diffracted-beam graphite monochromator, and scintillation counter. The cell was loaded into the diffractometer in such a way as to keep the cell level and attention was paid to avoid sample displacement error as much as possible. Figure 2 shows a schematic view of the experimental setup used. The in-situ cell was connected by lead wires to a computer-controlled potentiostat. Voltage profiles were programmed into the PC for variable voltage experiments or held at a constant voltage during static measurements. The current collector within the in-situ cell was used as an internal standard to correct for whatever sample displacement error occurred. Parameters for typical scans were a 34-80° 2θ range, 0.05° 2θ step-size, and varying count times ranging from 0.75 for some dynamic measurements to as long as 5 sec/step for the longer static-type measurements. The 34-80° 2θ range was chosen since the cell showed the greatest x-ray transparency over this angular range where reasonable diffraction data could be obtained. Smaller 2θ ranges were chosen in the case of some dynamic measurement scenarios.

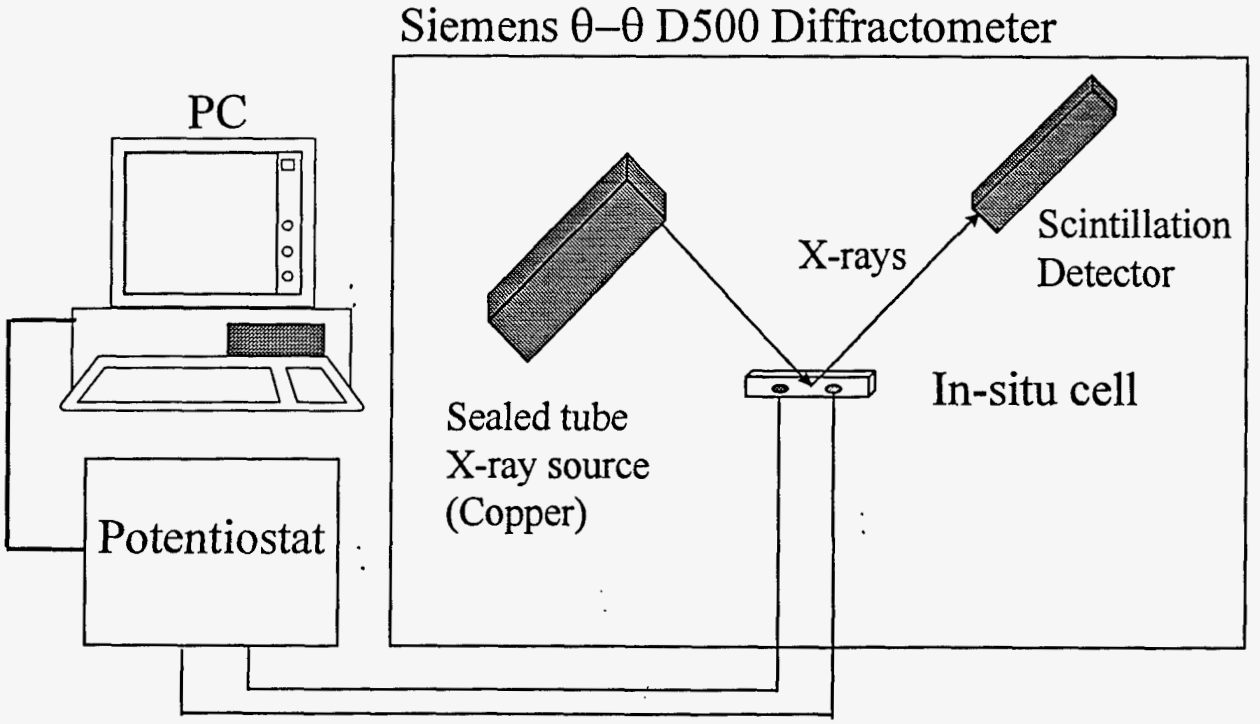

Figure 2: Schematic diagram of experimental setup for XRD employing in-situ cell.

RESULTS & DISCUSSION

Cell X-ray Transparency

The X-ray transparency of the in-situ cell is illustrated in Figure 3. This figure compares three diffraction patterns. The bottom pattern is that of a commercially available (FMC) $LiMn_2O_4$ spinel powder. This pattern is shown for comparison purposes. The middle pattern illustrates what the diffraction data looks like for a cathode prepared of this powder which has been placed within the in-situ cell bag but without any electrolyte added. It is clear that the pattern has not changed very much at all over the 34-80° 2θ range. This results indicates the ease of obtaining diffraction data from the material within the bag of the cell. Additional peaks from the aluminum current collector appear in the diffraction data since it has been placed on top of the cathode and is also detected during the scan. Since the structure and pattern for Al metal is well known, these peaks are very useful as an internal standard for the experiment. The top diffraction pattern was collected on an in-situ cell which was filled with electrolyte. In this case there does appear to be some attenuation of the diffraction data with the addition of the electrolyte. However, the diffraction peaks for both the aluminum and the spinel phase are easily detected above background with sufficient intensity to be used in both qualitative and quantitative type diffraction measurements.

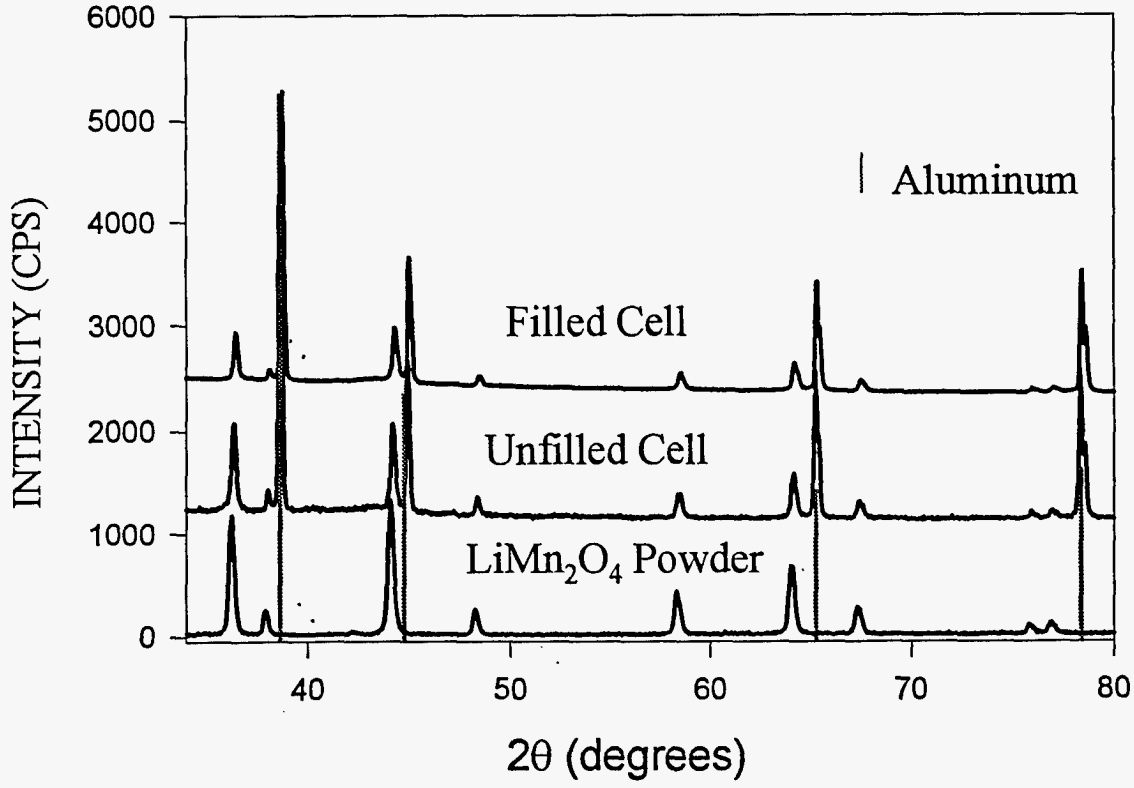

Figure 3: Illustration of X-ray transparency of in-situ cell. Bottom diffraction pattern shows typical XRD data for $LiMn_2O_4$ powder. Middle pattern shows diffraction data of cathode in the in-situ cell (no electrolyte); top pattern is diffraction data taken on in-situ cell with electrolyte.

Static Measurements on $LiMn_2O_4$

A series of diffraction scans on samples equilibrated at various voltage values are shown plotted with their cubic spinel lattice parameter vs. Li content (see Figure 4). The Li content was determined by first determining the quantity of Li in the initial starting powder by chemical analysis and then making the assumption that all the Li present is found as the spinel. The Li content was determined to be $Li_{1.2}Mn_2O_4$ by inductively coupled plasma (ICP). Using the initial value of the Li content, the reduction of Li in each cell was based on the capacity of each cell and the charge passed to reach equilibrium. Cells prepared using this powder were charged to various voltage values and then held constant at that voltage while diffraction data was collected. The peaks were fit to obtain d-spacings for the respective hkl's and a least square refinement was performed to obtain a lattice parameter for the cubic spinel structure. Figure 4 shows the results of these static measurements. It is evident that the unit cell shrinks nearly linearly with reduction of Li content. There does, however, appear to be a slight break in the linearity at about 0.8 Li; below 0.8 the slope is higher at about 0.24 Å/Li while above 0.8 Li the slope decreases to 0.14 Å/Li. This suggests that the behavior of Li intercalation is different in the two regions. Study of the behavior in $Li_xMn_2O_4$ is ongoing. Diffraction data for the lower Li contents (below 0.4 Li content) were difficult to obtain due to the breakdown of the solvent in the in-situ cell.

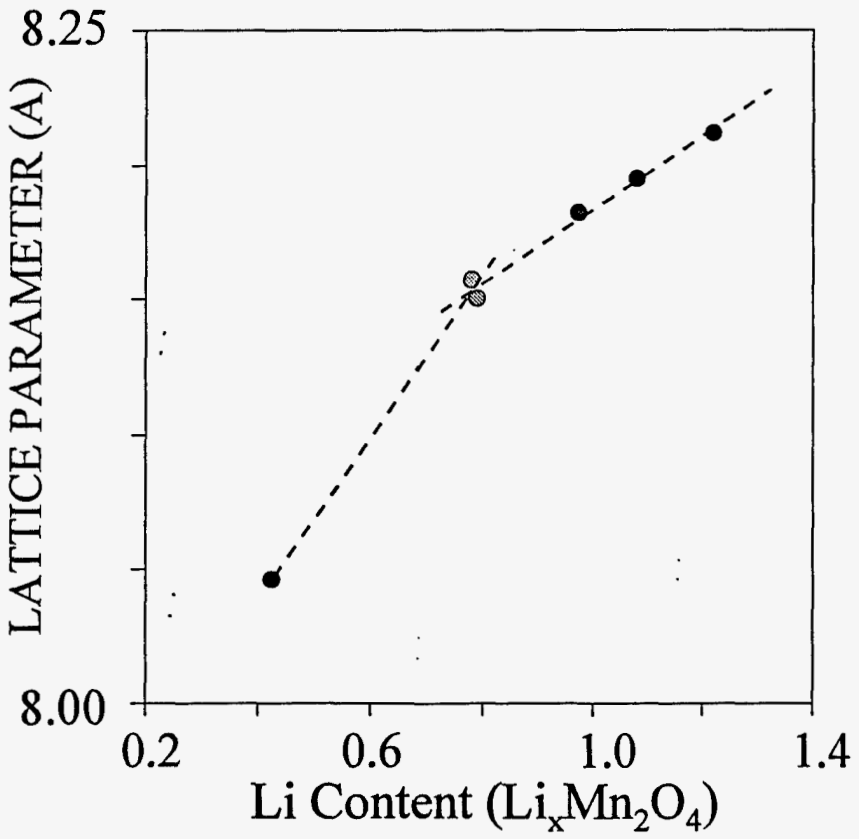

Figure 4. Dependence of lattice parameter on Li content in $LiMn_2O_4$ spinel.

Dynamic Measurements on $LiMn_2O_4$

As noted earlier, dynamic experiments can be used to detect changes of a material under non-equilibrium conditions. In one such experiment involving analysis of $LiMn_2O_4$, the diffraction data demonstrated interesting results when the cathode was charged and analyzed too quickly for equilibration at the designated voltage. Figure 5 shows the diffraction data for the 35-40° 2θ range on a cell charged to a series of voltage values but not allowed sufficient time to come to the equilibrium Li content for that voltage. What is observed in this case is the presence of varying compositions of Li within the spinel structure, which gives rise to a broadening of the $Li_xMn_2O_4$ peaks and ultimately an apparent phase separation. The phase separation is illustrated by formation of two peaks for the (311) reflection at about 4.06V (and possibly even three peaks by 4.24V). The phase separation concept was determined to be the best explanation for the observed data since other cubic spinel peaks recorded (but not shown) display the same peak separation behavior independent of their indexed (hkl) assignment. This is in contrast to the possibility that a phase transition occurred (e.g. change in lattice symmetry) in which case the peak splitting would have a marked dependency on a the (hkl) of each x-ray reflection.

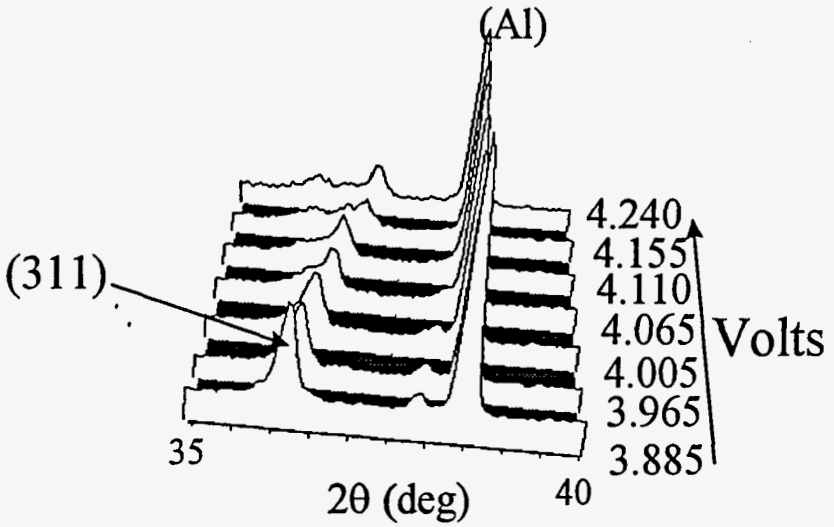

Figure 5. 3-D view of diffraction data for $LiMn_2O_4$ cathode monitored as a function of voltage. The (311) reflection for the spinel shows peak splitting consistent with a kinetically-controlled phase separation of the spinel structure into varying regions of Li content within the lattice.

Another example of a dynamic measurement is shown in Figure 6. In this experiment the cell was discharged from about 3.8V down the 3 volt plateau to 2V potentiodynamically, while a series of diffraction scans were collected. This analysis proved quite revealing; a phase transition is clearly seen occurring as the cell is forced to intercalate more and more Li. The observed reflections for the new structure match well with the tetragonal structure $Li_2Mn_2O_4$ reported by

Goodenough, *et al.*[5] This information concerning the structural transition of the spinel structure is important for understanding the potential usefulness and likely problems posed by employing the 3 volt plateau in battery development.

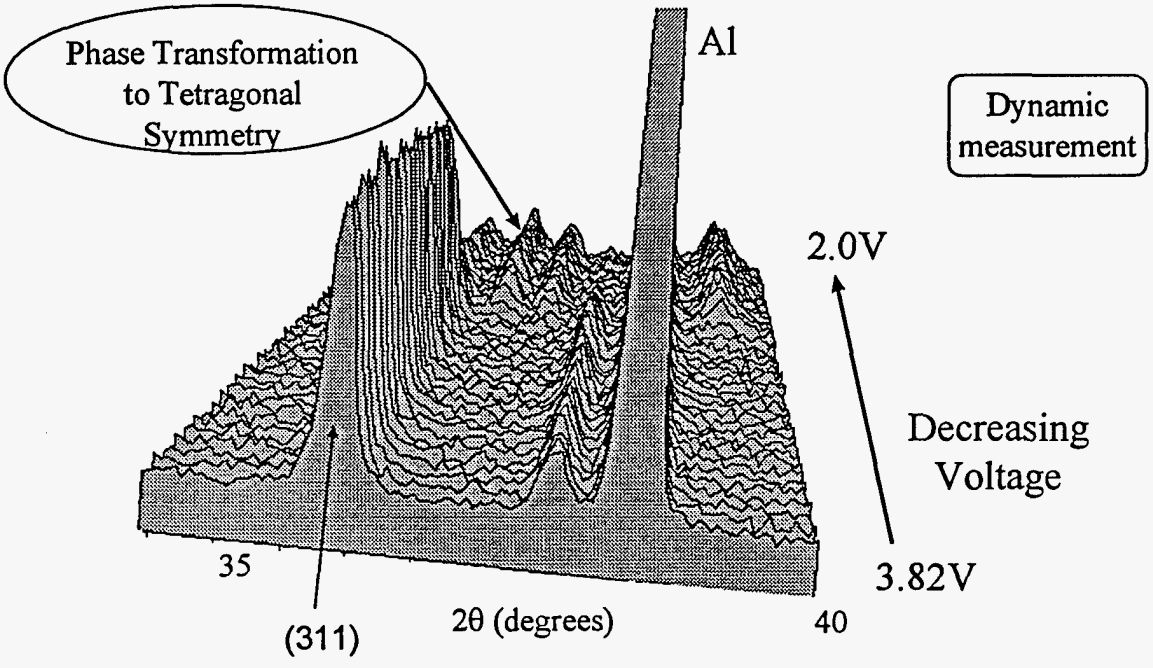

Figure 6. Potentiodynamic analysis gives an overview picture of structural distortions in $Li_{1+x}Mn_2O_4$ down the 3V plateau. As Li is added to lattice, eventually the structure undergoes a phase transition to a tetragonal phase.

Additional Materials

It was of considerable interest to determine if the use of the in-situ cell could be extended to investigations of other materials in both cathode and anode applications. The flexibility of the cell design makes analysis of either anode or cathode as easy as flipping the cell over and remounting it in the diffractometer. Just as the aluminum current collector could be used as an internal standard for the cathode, the anode current collector can also be used as the internal standard on the anode side. Figure 7 illustrates diffraction data collected on an anode of Lonza graphite. This graphite material displays a high degree of preferred orientation along the c-axis and hence has very strong (00*l*) reflections dominating the diffraction data. The bottom diffraction scan shows data for an initial cell prior to Li intercalation. The data shows very strong (002) and (004) graphite peaks, and additional peaks for nickel which was used as the anode current collector in this cell. Employing the nickel as an internal standard, the c-axis lattice parameter was calculated for the graphite material. Next, the cell was biased and Li was

intercalated into the graphite. The middle diffraction pattern shows the diffraction data for the Li-intercalated graphite. This pattern shows a very pronounced shift in the (00ℓ) graphite peaks to lower 2θ or higher d-spacings consistent with Li intercalating between the graphite sheets. The c-axis lattice parameter was expanded by more than 8% by the Li intercalation. Next, the cell was reversed biased and Li was de-intercalated from the graphite. The top diffraction pattern in Figure 7 shows the diffraction data after Li was removed. Recovery of the Li from the graphite lattice looked promising in that the c-axis lattice parameter calculated for final state was nearly identical the starting value.

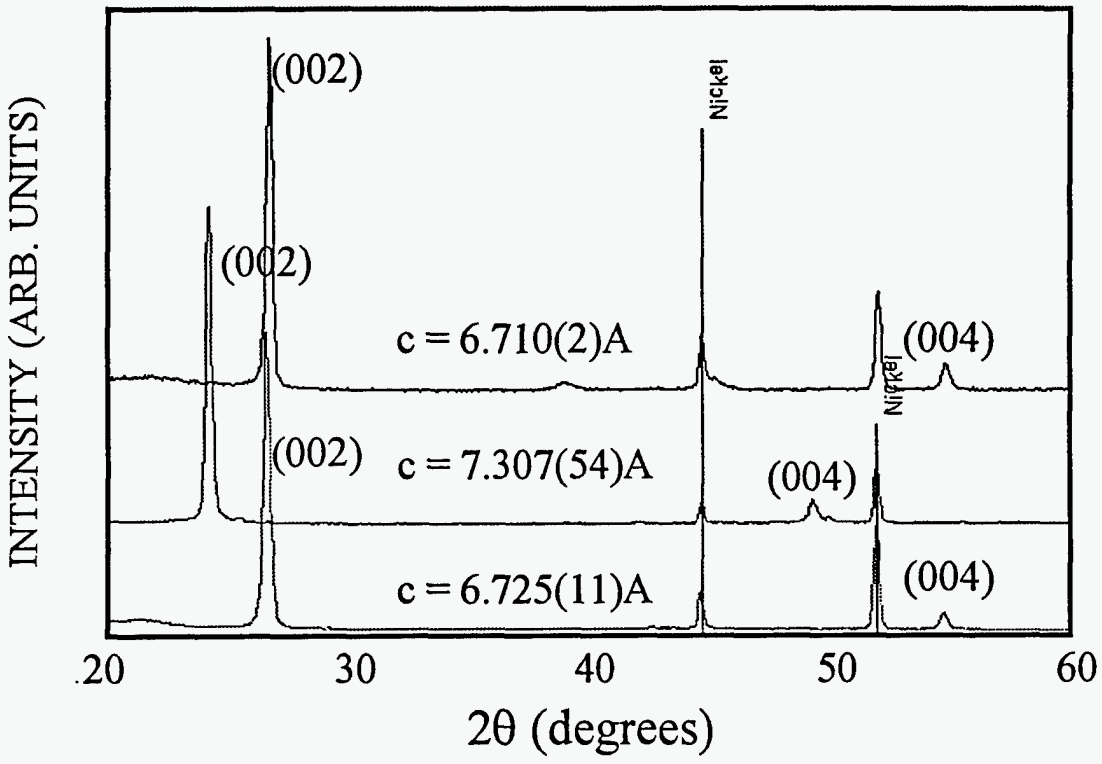

Figure 7. Diffraction data for graphite anode analyzed via the in-situ cell. Bottom pattern is initial scan of anode (Ni peaks from current collector). Middle scan is data on Li-intercalated graphite. Top scan is from anode after Li was de-intercalated back out of graphite.

Other cathode materials of interest in battery materials can be investigated using this in-situ cell. Successful in-situ XRD measurements have been performed on cells prepared with $LiCoO_2$ as the cathode material. Analysis of this cathode material is slightly more difficult since the cobalt has a tendency to display fluorescence during analysis which increases the background of the diffraction pattern. However, useful results have been obtained similar to the dynamic study shown in Figure 8. This 3-D graph shows the behavior of $LiCoO_2$ during charging. The initial peaks shown in the 48-62° 2θ range are consistent with the typical $LiCoO_2$ layered-type lattice.[5] Upon charging up the 4V plateau, Li is removed from the lattice and eventually the structure undergoes a phase transition indicated by the very dramatic peak shifts. The nature of this new lattice has not been fully determined at this time, but the results of a phase transition at low Li contents in $LiCoO_2$ have been predicted in computer modeling studies.[6]

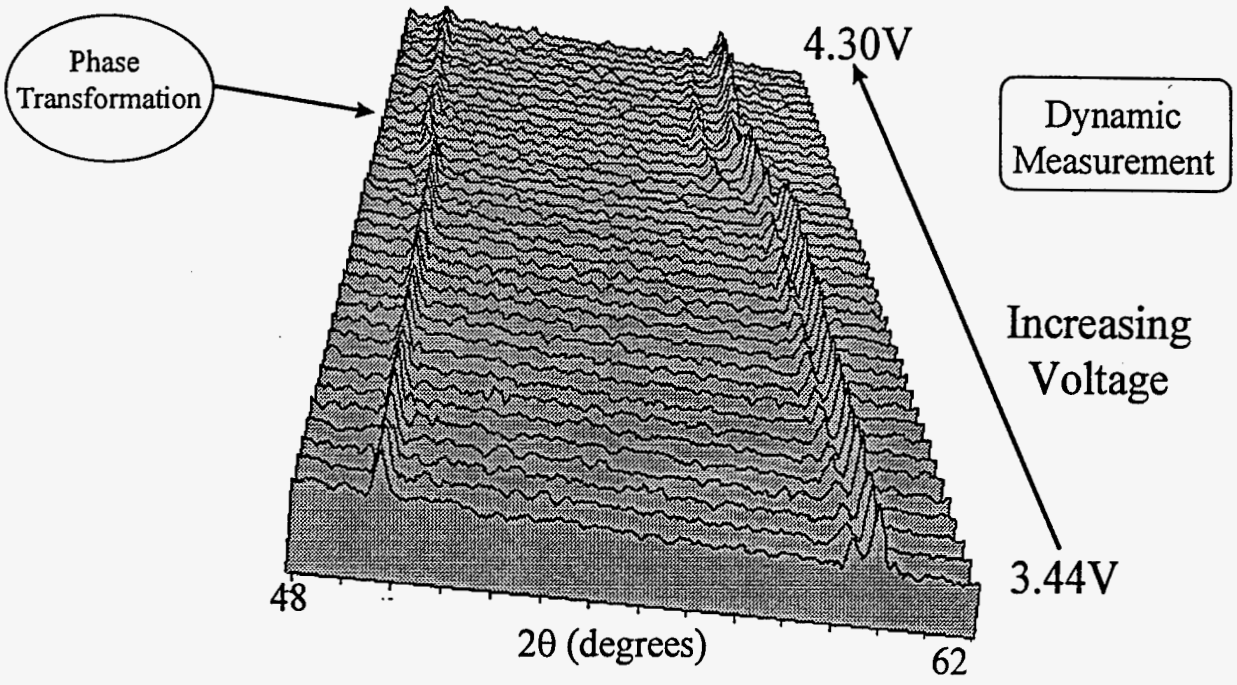

Figure 8. Dynamic study of $LiCoO_2$ using in-situ XRD cell. Upon charging, the $LiCoO_2$ undergoes a dramatic structural phase transition as Li is removed from the lattice.

CONCLUSIONS

In-situ XRD analysis is an excellent method for obtaining structural information in lithium battery development. Data can be either qualitative, such as phase formation and phase stability analysis, or quantitative, such as lattice parameter and kinetic behavior determination. Both the cathode and anode are easily analyzed, and the in-situ cell transparency to both light and x-ray wavelengths makes analysis straight-forward. In-situ studies may also be expanded to investigate new cathode/anode materials quickly and accurately.

ACKNOWLEDGMENTS

The authors would like to thank Jill Langendorf for her help with in-situ cell preparation. Sandia is a multiprogram laboratory operated by Sandia Corporation, a Lockheed Martin Company, for the United States Department of Energy under contract DE-AC04-94AL85000.

REFERENCES

1. D. Linden, editor, Handbook of Batteries, 2nd ed., McGraw Hill, New York, 1995.
2. M. N. Richard, I. Koetschau, and J. R. Dahn, *J. Electrochem. Soc.* **144** 554-557 (1997).
3. E. M. Levin, C. R. Robbins, H. F. McMurdie, Phase Diagrams for Ceramists, The American Ceramic Society, Columbus, OH, 1964, pp. 21.

4. J. Goodenough, M. Thackeray, W. David, and P. Bruce, *Rev. Chem. Miner.* **21** 435 (1984).
5. R. J. Gummow, M. M. Thackeray, W. I. F. David, and S. Hull, *Mat. Res. Bull.* **27** 327-337 (1992).
6. C. Wolverton, private communication.

Report Number (14) SAND--98-0408C
CONF-971201--

Publ. Date (11) 199802
Sponsor Code (18) DOE/ER, XF
JC Category (19) UC-400, DOE/ER

DOE